CALIFORNIA INSTITUTE OF TECHNOLOGY

SEISMOLOGICAL LABORATORY 252-21

June 27, 1997

ANNUAL PERFORMANCE REPORT

"Impact Cratering Calculations"
10/1/96-9/30/97

NASA/Goddard Grant NAG5-4206

Principal Investigator: Thomas J. Ahrens
Seismological Laboratory 252-21
California Institute of Technology
Pasadena, CA 91125
telephone# (626) 395-6906
fax# (626) 564-0715, 568-0935
e-mail: tja@caltech.edu

Distribution: Ms. Loren M. Sunell, Grants Officer (original)
Dr. Patricia Rogers, Technical Officer
NASA Center for Aerospace Information (reprod. copy)

ANNUAL RESEARCH REPORT
NASA Grant NAG-4206

I. INTRODUCTION

Understanding the physical processes of impact cratering on planetary surfaces and atmospheres as well as collisions of finite-size self-gravitating objects is vitally important to planetary science. The observation has often been made that craters are the most ubiquitous landform on the solid planets and the satellites. The density of craters is used to date surfaces on planets and satellites. For large ringed basin craters (e.g. Chicxulub), the issue of identification of exactly what "diameter" transient crater is associated with this structure is exemplified by the arguments of Sharpton et al. [1993] versus those of Hildebrand et al. [1995] . The size of a transient crater, such as the K/T extinction crater at Yucatan, Mexico, which is thought to be the source of SO_2-induced sulfuric acid aerosol that globally acidified surface waters as the result of massive vaporization of $CaSO_4$ in the target rock, is addressed by our present project.

The impact process excavates samples of planetary interiors. The degree to which this occurs (e.g. how deeply does excavation occur for a given crater diameter) has been of interest, both with regard to exposing mantle rocks in crater floors, as well as launching samples into space which become part of the terrestrial meteorite collection (e.g. lunar meteorites, SNC's from Mars). Only in the case of the Earth can we test calculations in the laboratory and field. Previous calculations predict, independent of diameter, that the depth of excavation, normalized by crater diameter, is $\overline{d_{ex}/D} = 0.085$ [O'Keefe and Ahrens, 1993]. For Comet Shoemaker-Levy 9 (SL9) fragments impacting Jupiter, predicted excavation depths of different gas-rich layers in the atmosphere, were much larger.

The trajectory and fate of highly shocked material from a large impact on the Earth, such as the K/T bolide is of interest. Melosh et al. [1990] proposed that the condensed material from the impact upon reentering the Earth's atmosphere induced. radiative heating, and producing global firestorms. The observed reentry splash of the SL-9 impact-induced plumes that reimpact Jupiter [Boslough et al., 1994] supported Melosh's K/T model.

The fate of early primitive planetary atmospheres during the latter stages of planetary accretion, resulting from impactors in the 10^0 to 10^3 km diameter require modeling, e.g. Newman et al. [1997]. Ahrens [1990; 1993] and Chen and Ahrens [1997] found that upon delivery of most of the impact energy to the solid planet, very large ground motions arise, which couple sufficient kinetic energy to the atmosphere to cause substantial atmospheric escape. The trade-off of this model with that of Cameron [1997] who suggests that atmospheric blow-off occurs as a result of the massive impact-induced heating of the atmosphere and Pepin [1997] who uses this heating event to model differential hydrodynamic loss of lighter atmospheric gases, requires further research.

a) Complex Multi-Ring Craters

We have continued to conduct cratering calculations on silicate surface out to very long times so as to model gravity driven crater oscillations [O'Keefe and Ahrens, 1997]. We used the Mohr-Coulomb pressure strength models for the strength, Y:

$$Y = Y_d + (Y_o - Y_d) \exp [(\partial Y/dP)\, P/(Y_o - Y_d)] \qquad (1)$$

where $(\partial Y/\partial P)_{p=o}$ is the initial Mohr-Coulomb slope and Y_o and Y_d is the STP and strength at depth. We took $Y_o = 0$ for the present studies. Also, we modeled fracturing and comminution using the Johnson-Cook [1985] approach. These different strength models resulted in significant differences in the final crater depth, diameter and other features.

Examples of simple bowl shaped, incipient flat floored and complex crater calculations are shown in Figures 1, 2, 7, and 8. A parameter that determines the crater morphology is the normalized strength, $Y/\rho g d_p$, where Y is planetary strength, g is the planetary gravity and d_p is the depth of penetration under zero strength conditions [O'Keefe and Ahrens, 1993]. When $Y/\rho g d_p >> 1$, the impact produces simple craters and when $Y/\rho g d_p << 1$, the impact produces centerline oscillations and complex craters.

We find that the maximum depth of penetration is given by

$$d_p = 0.83\ (\rho/\delta)^{-0.26}/(ga/U^2)^{0.22} \quad (2)$$

where ρ and δ are the density of the target and impactor, respectively, and "a" is impactor radius.

Moreover, the maximum diameter of the transient crater is

$$D_p/a = 0.22\ (\delta/\rho)^{0.26}/\ (ga/U^2)^{0.22} \quad (3)$$

For the Earth, impacted by a 10 km diameter projectile, we obtain the diameter of the inner ring (applicable to Chicxulub) as

$$D_{ir} = 0.39\ D_p \quad (4)$$

and

$$d_p = 0.4\ D_{ir} \quad (5)$$

The description of a complex crater (Figs. 7 and 8) uses tracer particles to delineate the effect of the crater motions on the deformation of the planet's stratigraphy, e.g., Fig. 7a. The time is normalized by dividing by (a/U). In Fig. 8b, the oscillating peak has formed and is at its first maximum height. The crater lip, with inverted stratigraphy, formed during excavation of the transient crater. During the formation of the transient centerline peak, the stratigraphy is rotated 90 deg. within the transient cavity. The first peak collapses and forms a second (shallower) transient crater cavity. The stratigraphy near the centerline maintains its pre-impact ordering, whereas the stratigraphy, in the "vertical ring region" is rotated by 90 degrees. This ring forms because of greater shock heating, plastic work, fracture and comminution weakness of this zone, relative to the material at the base of the transient peak. The second transient cavity rebounds and produces a small narrow second centerline peak; this decays to give a central structure. In the case shown here a small centerline peak and ring formed. This ring does not have a rotated stratigraphy in contrast to the "vertical ring". The final crater are shown in Figs. 7e and 7f.

The maximum depth of penetration and the magnitude of the peak oscillation are given in Fig. 3. The transition (Fig. 5) between simple and complex craters occurs for $Y/\rho g d_p \sim 1$.

We estimate the strength at depth by using the relationship between the depth of penetration and the above transition condition. Thus $Y = 0.04\rho g D_{ir}$ (Fig. 6). In the case of impacts on the Earth, for an inner ring diameter of 100 km, the strength, at depth, is ~700 MPa.

The above scaling relations can be applied to the Chicxulub impact. The inner ring diameter is estimated as 90 to 105 km [Hildebrand et al., 1991]. This implies that the maximum depth of penetration was ~40 km (Fig. 3). From Fig. 4, we find for an asteroid impact at 20 km/s, or a comet impact at 40 km/s, the impactor diameter is ~14 km. For a comet at 60 km/s, the impactor diameter is ~12 km.

We are now able to describe the evolution of the depth, diameter, and crater lip height of transient craters, as well as gravitational collapse of large craters as a function of density, crustal strength, planetary gravity, and impact velocity. In Fig. 8, we show cross-sections of a crater induced by the impact of a silicate impactor with a radius (a) of 50 km at a velocity (U) of 12 km/sec. We chose this speed to minimize vaporization. The cratering flow is given for an unprecedented time duration, for Ut/a = 463, the equivalent real time is 32 minutes!

b) Impact on Asteroids and Asteroidal Break-up

Asteroid Breakup

The collisional evolution of the asteroids is previously modeled by analogy with small-scale, strength dominated laboratory impact experiments. However, recent calculations by Holsapple [1993] suggest that gravity dominates over strength in determining impact behavior for silicate objects larger than ~6 km diameter. Moreover, a recent study by Nolan et al. [1996] argued that for impacts on asteroids by projectiles with diameters greater than $\sim 10^2$ m, the

impact-induced shock wave fragments the pre-existing solid rock prior to cratering. Thus gravity rather than strength plays a role even for impacts at small scales on asteroids. Therefore strength-dominated impacts may not apply to most numbered asteroids or to most meteorite parent bodies.

To investigate the impact response of fragmented asteroids, we used the Caltech three-dimensional Smoothed Particle Hydrodynamics (SPH) computer code that includes a rigorous treatment of gravity and studied collisions at impact speeds of 3-7 km/s and angles of 15 to 75°. We calculated the catastrophic threshold (Q^*) for 50% target mass removal occurs at projectile kinetic energy per unit target mass (specific energy) equal to be 10^4 to 10^6 J/kg for target diameters of 10 to 10^3 km, respectively [Love and Ahrens, 1996].

Upon extrapolating to smaller sizes, a new estimate is obtained of the asteroid diameter marking the boundary between strength and gravity dominance for impact cratering: 250± 150 m (Fig. 9).

Asteroid Rotation.

The rotation rates of the asteroids are deduced from light curves. We studied oblique impacts at 5 km/sec on solid (and porous) rock targets in the 10 - 10^3 km diameter range with rock impactors in the 0.8 to 470 km diameter range. The effectiveness of the target in acquiring spin angular momentum is expressed as the fraction, ζ, of the system angular momentum prior to collision that is retained by the target. Small scale experiments including our own (e.g. Yanigasawa et al. [1991]) yield values of $\zeta \cong 0.1$ to 0.7, previous theoretical estimates assumed values of $\zeta = 0.01$-0.3, whereas using our SPH results [Love and Ahrens, 1997] yielded even lower values, i.e. $\zeta = 0.01$ to 0.1.

The rotation of a collisionally mature asteroid is the result of a 'random walk' of many impacts. Applying the present model to observed asteroid rotation rates is an approximation, because it neglects initial target spin and only shows the effect of a single impact rather than the sum of many. Initial spin, however, has only a minor effect on mass ejection. Furthermore, if impacts occur at random orientations, the effects of initial target rotation may average to zero. Combining the curve in Fig. 10a with the observation that target mass removal is proportional to impactor mass for a given target size and including the impactor mass distribution allows us to compare the importance of different sized impacts in controlling asteroid spin (Fig. 10b). Small erosive events are frequent but have little effect on the spin. Impacts removing more than ~0.75 of the target's mass alter rotation significantly, but not enough to compensate for their rarity. Between those extrema, occasional catastrophic impacts leaving remnants with 0.40-0.65 of their original masses are the most effective in determining asteroid rotation rates and thus represent the 'step size' of the random walk. We find such impacts produce (on initially non-rotating targets) spin rates of 1.8-4.2d^{-1}. This is consistent with the ~2.5d^{-1} observed asteroidal mean rotation rate.

The line at the top of Fig. 10a indicates an equatorial rotation velocity equal to the low orbit velocity. This is the rotational breakup for strenghless gravitating objects. For a sphere, the breakup spin rate (in d^{-1}) is given by $f_{max} = 86{,}400 \sqrt{G\rho/3\pi}$, where ρ and G are the density and the gravitational constant in mks units. For increasingly large impacts, final spin rates approach, but do not reach, the breakup limit.

The observed mean spin frequencies of C-, S- and M-class asteroids (2.2d^{-1}, 2.5d^{-1} and 4.0 d^{-1}, respectively) fall in nearly the same proportion as the square roots of their presumed densities (~2,000 kg m^{-3} for the 'carbonaceous' C class, ~2,700 kg m^{-3} for the S class, and ~7,800 kg m^{-3} for the 'metallic' M class). We speculate that collisionally mature Kuiper-belt objects (ρ~1,00 kg m^{-3}) should have a mean spin rate near 1.5d^{-1}.

c) Impact Erosion of Planetary Atmospheres

Cameron [1983] suggested that large impacts onto planetary atmospheres may induce atmospheric ejecta that escapes the planet. Hence, impacts can erode planetary atmospheres. Melosh and Vickery [1989] developed a semianalytic model applicable to impactors with radii, that are small compared to that of a planet, developed a physical model describing this process (and applied it to Mars), whereas Zahnle et al. [1992] applied this concept to planetary satellite atmospheres. Recently, Cameron [1997] has also shown that for giant impacts on the Earth, concurrent atmospheric heating causes thermal atmosphere escape.

Our group has begun [Ahrens, 1993] to study the atmospheric erosive regime for impactors with diameters greater than the atmospheric scale height, but substantially less than the diameter of the target planet. In this regime (Fig. 11) a larger-sized projectile passes through the atmosphere (depositing only a few percent of its energy [O'Keefe and Ahrens, 1982]) and induces a strong shock wave within the solid Earth (or other planet). This shock wave upon reflecting at the solid planet-atmosphere interface gives rise to an upward driven shock in the atmosphere. This shock increases its shock and particle velocity with altitude such that the escape velocity is exceeded at high altitude and the atmosphere is eroded [Chen and Ahrens, 1997]. To study this problem we modified a compressible flow, LaGrangian one-dimensional finite difference code [Kipp and Lawrence, 1982] to include gravity and obtained particle velocity profiles (e.g. Fig. 12).

Our second approach was our analytic and finite difference investigation of a near-surface explosion (as a proxy for an impact) at the base of an exponential atmosphere [Newman et al., 1997]. Here the streamlines of the particle velocity induced in the atmosphere for a surface explosion are (for the first time) analytically calculated. This model yields less gas loss via atmospheric escape than the Melosh and Vickery model. The Melosh and Vickery [1989], Chen and Ahrens [1997], and Newman et al. [1997] approaches all suffer from the neglect of the downward flow-field set-up by the incoming bolide before impact with solid planet. Moreover, the Newman et al. model has been run only for cases, where the energies are similar to the K/T bolide (5×10^{30} erg).

d) Impact of Comet Shoemaker-Levy 9 (SL9) on Jupiter.

We finished publication of our initial attempts to conduct a full three-dimensional smoothed particle hydrodynamic description of the impact of SL9 fragments on Jupiter. We also conducted a new analysis of methods of scaling impact events so as to understand why the plume heights reported by Hammel et al. [1995] were nearly constant varying from 2700± 170 to 3350 ± 170 km above the 1 bar level whereas the mass (and energy) of the fragments appeared [Weaver et al., 1995] to vary by a factor of 20!

We developed a semianalytic model for the breakup of fragments of SL9 on entry into Jupiter's atmosphere [Roulston and Ahrens, 1997]. We assume the impacting fragments behaved as viscous fluid and their breakup resulted from growth of hydrodynamic instabilities. The wavelength of the smallest instabilities that contribute to mass loss determines the depth of penetration, which is consistent with the changes in penetration depth obtained using numerical models with different resolutions. If the diameter of the impactor corresponds to 8 resolution elements then the penetration depths obtained are about 10^2 km too great. To obtain penetration depths within one scale height (≈25 km) of the viscosity limited value, at least 25 resolution elements are required across the diameter of the impactor in agreement with the studies of K. Zahnle and M.-M. MacLow [1994]. This argument indicates that the zoning of several groups, that conducted SL9 impact calculations, including our own, was too coarse! We show that two different regimes of hydrodynamic mass loss exist, one caused by Kelvin-Helmholtz (KH) type instabilities and a later one caused by the onset of Rayleigh-Taylor (RT) type instabilities. These regimes can be identified in the numerical results of D. A. Crawford et al. [1994], where KH instabilities appear to be the major mass loss mechanism between 100 and 200 km (below 1 bar) and RT instabilities become dominant below 200 km (below 1 bar).

The upward velocity of material behind the shock caused by the expansion of the superheated gas in the comet's wake is then calculated and shown to be about 12 km sec^{-1} and, to

a first approximation, independent of the impacting fragment size provided that the fragment is not significantly decelerated, upon initial entry, before it reaches the altitude (100 mbar) tropopause. This upward velocity implies a plume height of 3000 km above the 1-bar level, which agrees with Hammel et al.'s [1995] observations. It is shown that for no significant deceleration to occur before the tropopause, the impacting fragments that produced plumes must have had diameters larger than 0.3 km. This, in turn, implies a progenitor diameter of 1.6 km (in agreement with pre-impact calculations of Scotti and Melosh [1993], Asphaug and Benz [1994], and Solem [1994]). It is then estimated that the time interval between impacts of 0.3 km diameter comets on Jupiter is approximately 500 years, whereas the interval between the impact of 1.6 km comets is about 6000 years.

The chemical abundances in the plumes, especially their high CO content, indicate that the fragments contain primitive materials and thus SL9 was probably originally a Jupiter family comet. As can be seen in our calculated color image of the plume cross-section (123 sec after impact) the visible plume, probably dark from carbon originating in shock processed CH_4 rich-stratosphere (blue) [Takata et al., 1995], attenuates the line emission from cometary species (red triangles). Our simulations [Takata and Ahrens, 1997] suggest that the energy source that produce the observable waves [Ingersoll and Kanamori, 1995] is located in the stratosphere, rather than in the deep troposphere. Finally, the ejecta pattern observed overlying the clouds, were simulated by the ejection of atmospheric gas and cometary materials from a narrow ~30° cone region along the trajectory.

REFERENCES

Ahrens, T. J., Earth Accretion, in *Origin of the Earth*, edited by J. Jones and H. Newsom, pp. 211-227, Oxford U. Press, Oxford, 1990.

Ahrens, T. J., Impact erosion of terrestrial planetary atmospheres, *Annu. Rev. Earth Planet. Sci.*, *21*, 525-555, 1993.

Ahrens, T. J., and J. D. O'Keefe, Impact of an asteroid or comet in the ocean and extinction of terrestrial life, *Proc. Lunar & Planet Sci. Conf. XIII, Part 2, J. Geophys. Res. Suppl.*, *88*, A799-A806, 1983.

Asphaug, E., and W. Benz, Density of Comet Shoemaker-Levy 9 deduced by modeling breakup of the parent rubble-pile, *Nature*, *370*, 120-124, 1994.

Boslough, M. B., D. A. Crawford, A. C. Robinson, and T. C. Trucano, Mass and penetration depth of Shoemaker-Levy 9 fragments from time resolved photometry, *Geophys. Res. Lett.*, *21*, 1555 - 1558, 1994.

Cameron, A. G. W., Origin of the atmospheres of the terrestrial planets, *Icarus*, *56*, 195-201, 1983.

Cameron, A. G. W., The origin of the Moon and the single impact hypothesis, V, *Icarus*, *126*, 126-137, 1997.

Chen, G. Q., and T. J. Ahrens, Erosion of terrestrial planet atmosphere by surface motion after a large impact, *Physics of the Earth and Planetary Interiors*, *100, Nos. 1-4*, 21-26, 1997.

Crawford, D. A., M. B. Boslough, T. G. Trucano, and A. C. Robinson, The impact of Comet Shoemaker-Levy 9 on Jupiter, *Shock Waves*, *4*, 47-50, 1994.

Davis, D. R., E. V. Ryan, and P. Farinella, Asteroid collisional evolution: Results from current scaling algorithms, *Planet. Space Sci.*, *42*, 599-610, 1994.

Farinella, P., P. Paolicchi, and V. Zappala, The asteroids as outcomes of catastrophic collisions, *Icarus*, *52*, 409-433, 1982.

Hammel, H. B., R. F. Beebe, A. P. Ingersoll, G. S. Orton, J. R. Mills, A. A. Simon, P. Chodas, J. T. Clarke, E. DeJong, T. E. Dowling, J. Harrington, L. F. Huber, E. Karkaoschka, C. M. Santori, A. Toigo, D. Yeomans, and R. A. West, Hubble space telescope imaging of Jupiter: Atmospheric phenomena created by the impact of Comet Shoemaker-Levy-9, *Science*, *267*, 1288-1296, 1995.

Hildebrand, A. R., G. T. Penfield, D. A. Kring, M. Pilkington, A. Z. Camargo, S. B. Jacobsen, and W. V. Boynton, Chicxulub crater: A possible Cretaceous-Tertiary boundary impact crater on the Yucatan Peninsula, Mexico, *Geology*, *19*, 867-871, 1991.

Hildebrand, A. R., M. Pilkington, M. Connors, C. Ortizaleman, and R. E. Chavez, Size and structure of the Chicxulub crater revealed by horizontal gravity gradients and cenotes, *Nature*, *376*, 415-417, 1995.

Holsapple, K. A., The scaling of impact processes in planetary sciences, *Ann. Rev. Earth Planet. Sci.*, *21*, 333-373, 1993.

Holsapple, K. A., Catastrophic disruptions and cratering of solar system bodies: a review and new results, *Planet. Space Sci.*, *42*, 1067-1078, 1994.

Housen, K. R., and K. A. Holsapple, On the fragmentation of asteroids and planetary satellites, *Icarus*, *84*, 226-253, 1990.

Ingersoll, A. P., and H. Kanamori, Waves from the collision of Comet Shoemaker-Levy 9 with Jupiter, *Nature*, *374*, 706-708, 1995.

Johnson, G. R., and W. H. Cook, Fracture characteristics of three metals subjected to various strains, strain rates, temperatures and pressures, *Eng. Fract. Mech.*, *21*, 1985.

Kipp, M. E., and R. J. Lawrence, WONDY V - A one-dimensional finite-difference wave propagation code, SAND 81-0930, Sandia Report, 1982.

Love, S., and T. J. Ahrens, Catastrophic impacts on gravity dominated asteroids, *Icarus*, *124*, 141-155, 1996.

Love, S., and T. J. Ahrens, Origin of asteroid rotation rates in catastrophic impacts, *Nature*, *386*, 154-156, 1997.

Melosh, H. J., N. M. Schneider, K. J. Zahnle, and D. Latham, Ignition of global wildfires at the Cretaceous/Tertiary boundary, *Nature*, *343*, 251-254, 1990.

Melosh, H. J., and A. M. Vickery, Impact erosion of the primordial Martian atmosphere, *Nature*, *338*, 487-489, 1989.

Newman, W., E. M. D. Symbalisty, T. J. Ahrens, E. Jones, and A. Chaikin, Impact events and the erosion of planetary atmospheres: Some surprising results from theory and simulation, *Icarus*, [Submitted], 1997.

Nolan, M. C., E. Asphaug, H. J. Melosh, and R. Greenberg, Impact craters on asteroids: Does gravity or strength control their size, *Icarus*, *124*, 359-371, 1996.

O'Keefe, J. D., and T. J. Ahrens, The interaction of the Cretaceous-Tertiary extinction bolide with the atmosphere, ocean, and solid earth, in *Geological Implications of Impacts of Large Asteroids and Comets on the Earth*, edited by L. T. Silver and P. H. Schultz, pp. 103-120, Geol. Soc. Amer. Spec. Paper 190, 1982.

O'Keefe, J. D., and T. J. Ahrens, Planetary cratering mechanics, *J. Geophys. Res.*, *98*, 17011-17028, 1993.
O'Keefe, J. D., and T. J. Ahrens, Complex craters: Relationship of peak rings to the impactor parameters, *J. Geophys. Res.*, to be submitted, 1997.
Pepin, R. O., Evolution of Earth's noble gases: Consequences of assuming hydrodynamic loss driven by giant impact, *Icarus*, *126*, 148-156, 1997.
Roulston, M., and T. J. Ahrens, Impact mechanics and frequency of SL9-type events on Jupiter, *Icarus*, [126], 138-147, 1997.
Scotti, J. V., and H. J. Melosh, Estimate of the size of Comet Shoemaker-Levy 9 from a tidal breakup model, *Nature*, *365*, 733-735, 1993.
Sharpton, V. L., K. Burke, A. Camargozanoguera, S. A. Hall, D. S. Lee, and et al., Chicxulub multi-ring impact basin - size and other characteristics derived from gravity analysis, *Science*, *261*, 1564-1567, 1993.
Solem, J. C., Density and size of Comet Shoemaker-Levy 9 deduced from a tidal breakup model, *Nature*, *370*, [6488], 349-351, 1994.
Takata, T., and T. J. Ahrens, Impact of Comet Shoemaker-Levy 9-Size, origin, and plumes-comparison of numerical analysis with observations, *Icarus*, *125*, [2], 317-330, 1997.
Takata, T., T. J. Ahrens, and A. W. Harris, Comet Shoemaker-Levy 9: Fragment and progenitor impact energy, *Geophys. Res. Lett.*, *22*, 2433-2436, 1995.
Vickery, A. M., and H. J. Melosh, Atmospheric erosion and impactor retention in large impacts, with applications to mass extinctions, in *Global Catastrophes in Earth History*, edited by V. L. Sharpton and P. D. Ward, pp. 289-300, Geol. Soc. Am. Special Paper 247, 1990.
Weaver, H. A., P. D. Feldman, M. F. Ahearn, C. Arpigny, and R. A. Brown, Hubble-Space Telescope observations of Comet-P/Shoemaker-Levy 9 (1993e), *Science*, *263*, 787-791, 1995.
Yanagisawa, M., J. Eluszkiewicz, and T. J. Ahrens, Angular momentum transfer in oblique impact, *Icarus*, *94*, 272-282, 1991.
Zahnle, K., and M. M. MacLow, The collision of Jupiter and Comet Shoemaker-Levy 9, *Icarus*, *108*, 1-17, 1994.
Zahnle, K., J. B. Pollack, and D. Grinspoon, Impact-generated atmospheres over Titan, Ganymede, and Callisto, *Icarus*, *95*, 1-23, 1992.

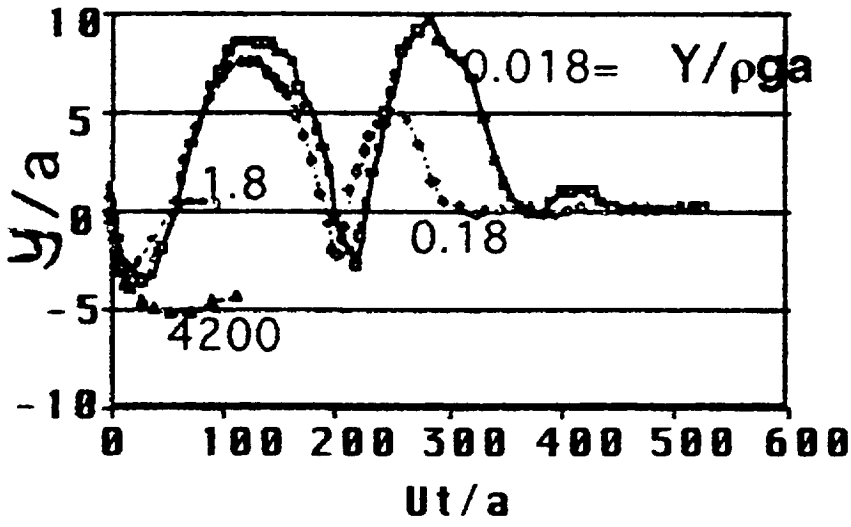

Figure 1. Time history of the interface between the impactor and the planet along the centerline of impact. Time is nondimensionalized by Ut/a. This figure illustrates the evolution of the depth of penetration and the peak oscillations depend on the ratio of Tresca crustal strength, Y, gravity, g, and projectile radius values, or, Y/ρga are shown for each curve.

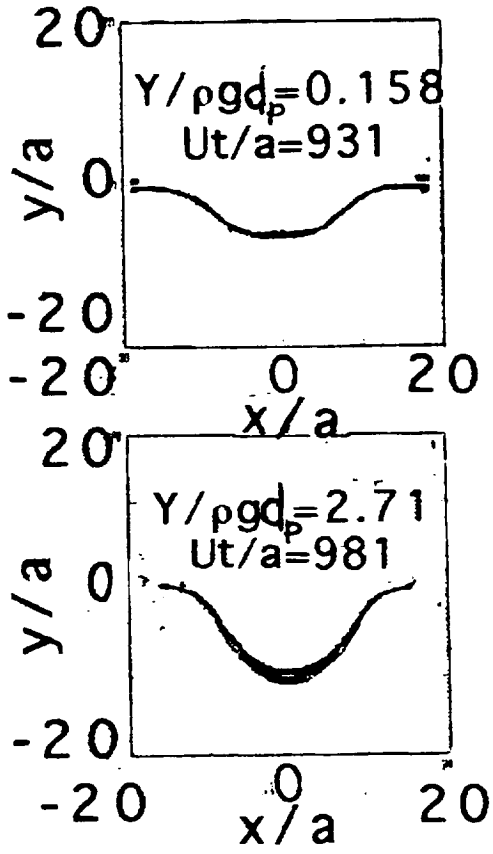

Figure 2.Simple (lower) bowl and flat floored (upper) shaped craters profiles for two different strength crusts. Here d_p is the maximum depth of penetration of impactor for Earths gravity, for $Y/\rho g d_p = 2.71$ case at Ut/a = 981, for a 50m radius silicate, 12km/sec impactor, crater is formed in 40 secs. For $Y/\rho g d_p = 0.158$ case at Ut/a = 931 crater is also formed in 40 secs.

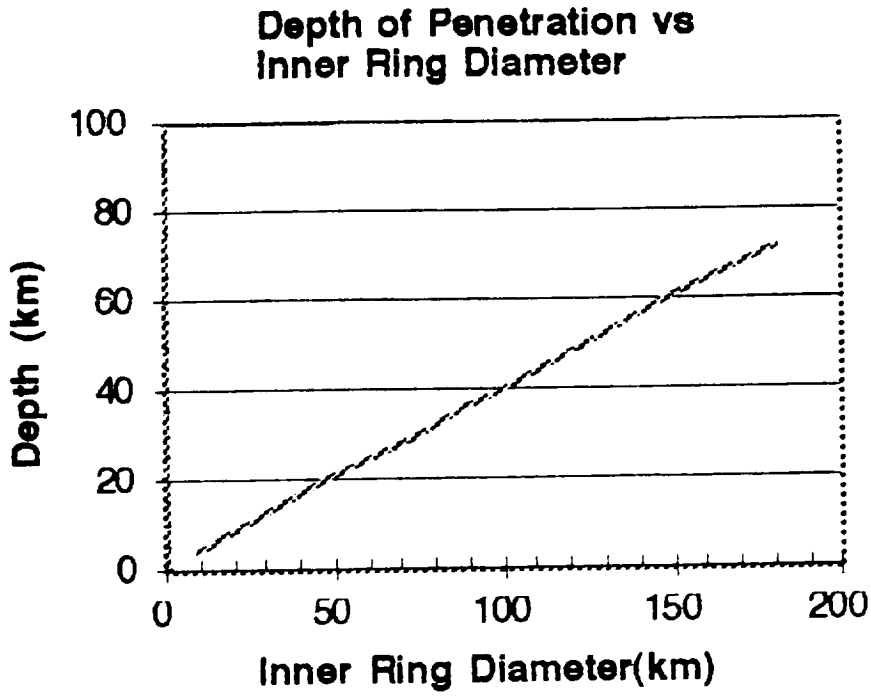

Figure 3. Depth of penetration as a function of inner ring diameter.

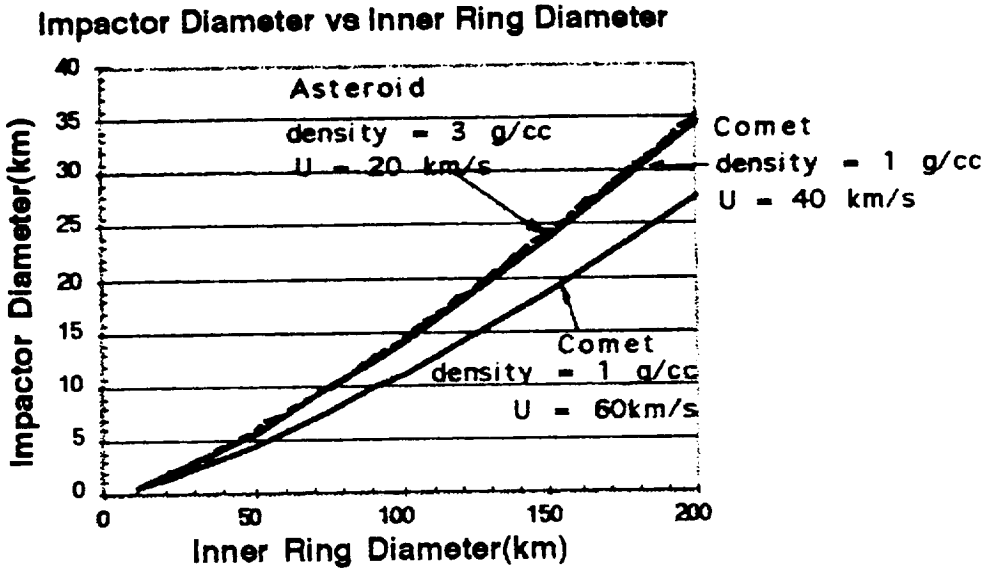

Figure 4. Impactor diameter as a function of inner ring diameter for different impactors.

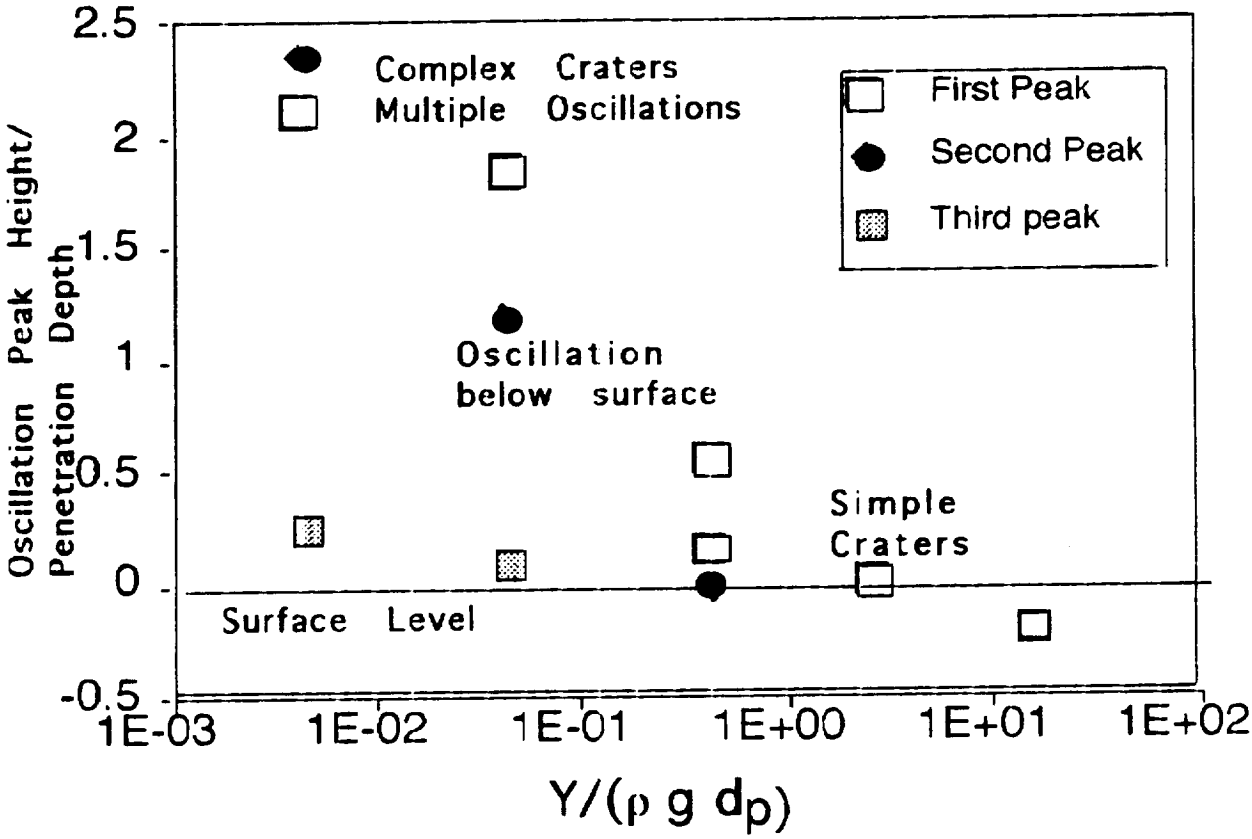

Figure 5.Centerline oscillations amplitude versus strength parameter. Simple craters formed in strong media (right) produce only one peak, whereas, impact into weak media induce three or more oscillations (left).

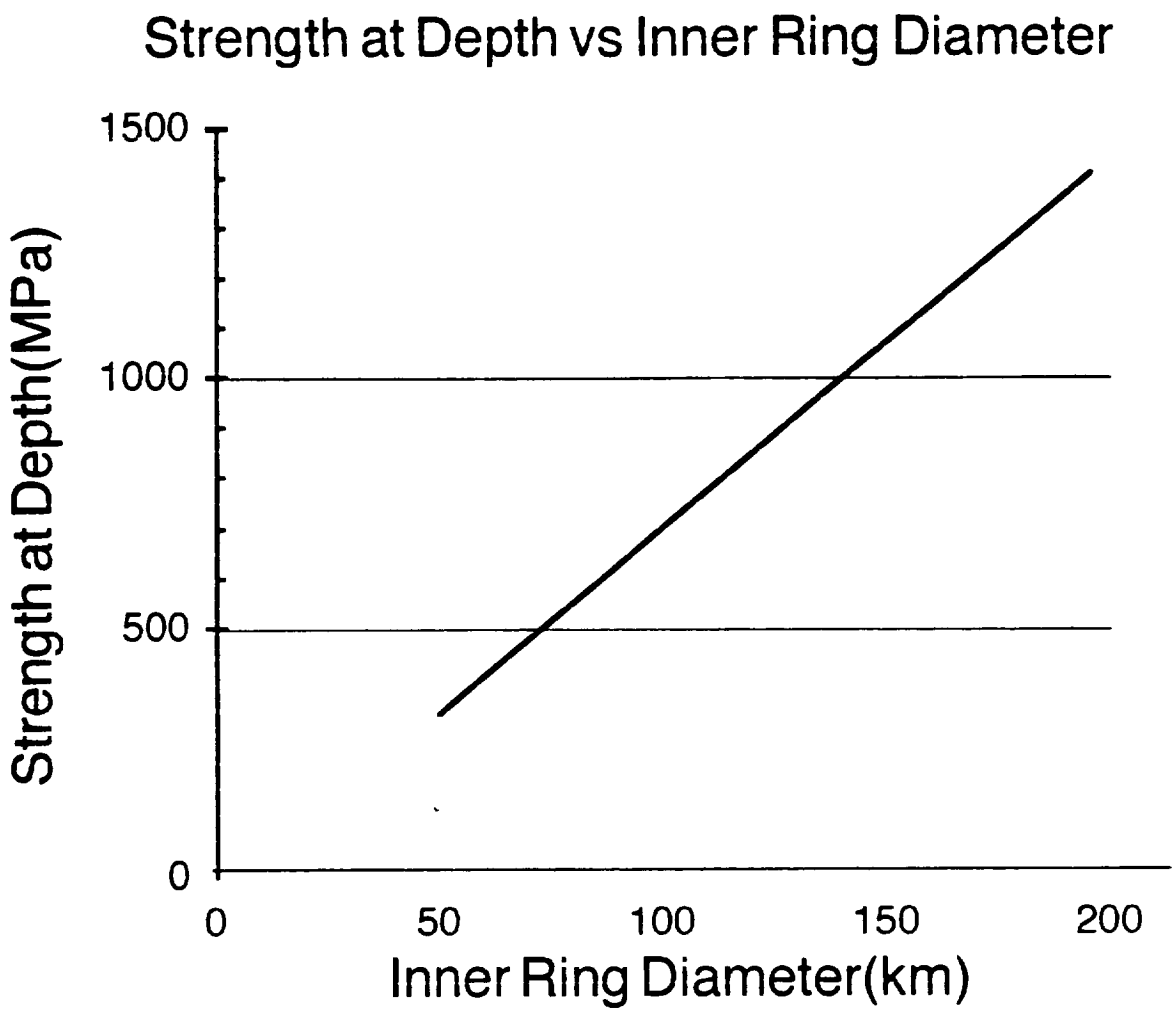

Figure 6. Final crater inner ring diameter versus near-surface planetary strength for a Chicxulub energy impact event.

TJA97035SFD

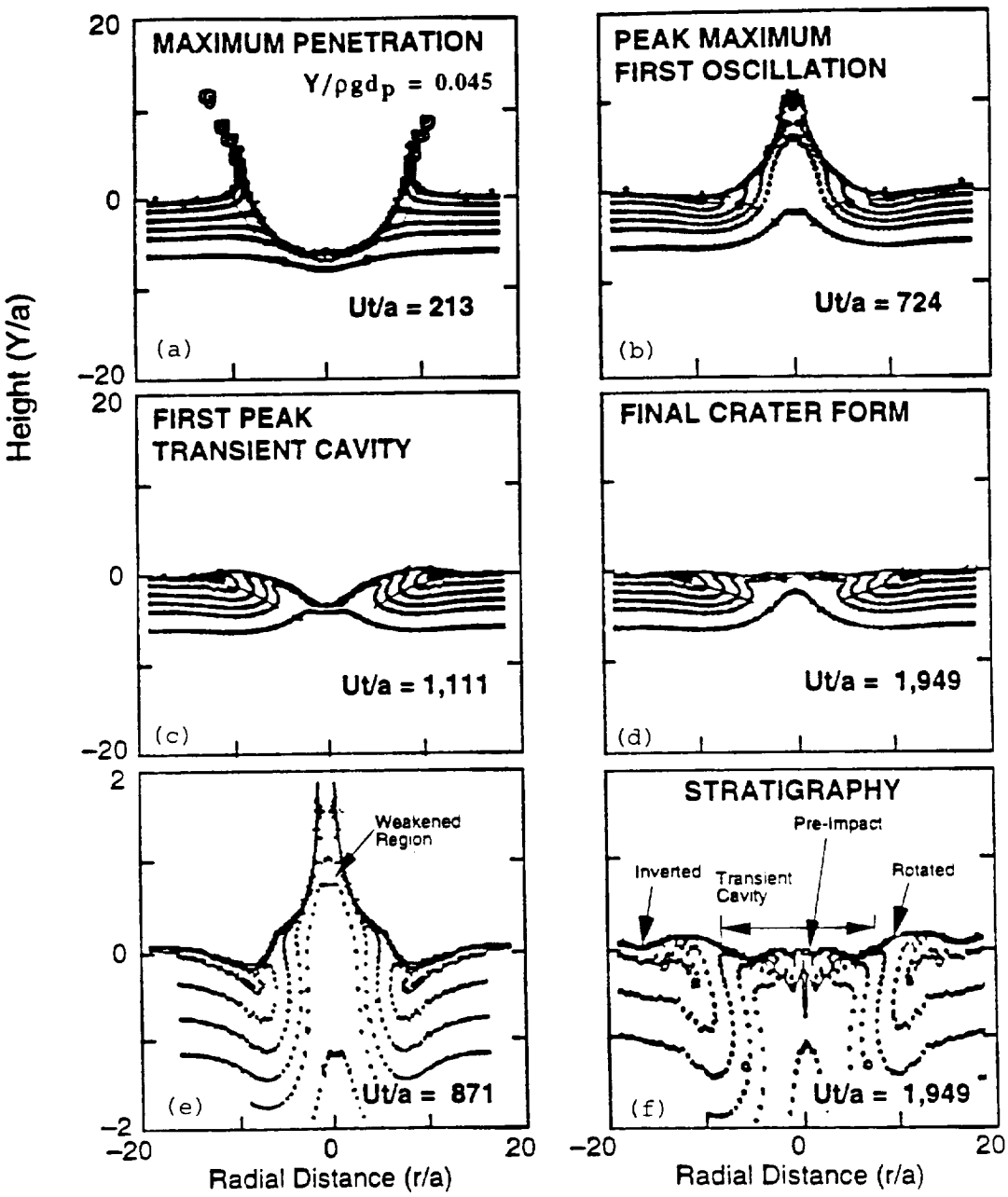

Figure 7. Complex crater evolution. Note expanded vertical scale in e and f.

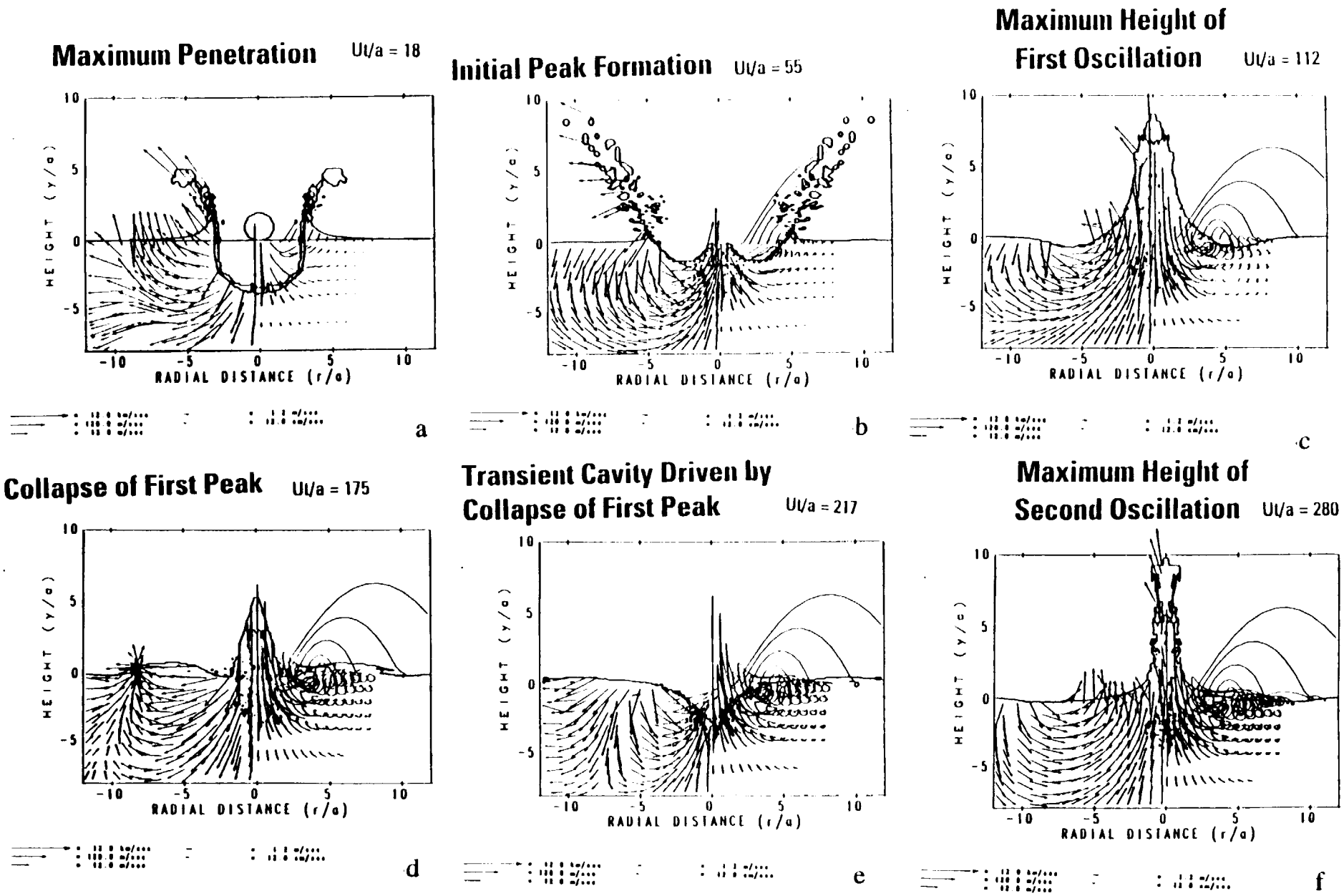

Figure 8 Impact induced flow for 12 km/sec silicate impactor upon a low strength silicate half-space. Left side of panels indicate particle velocity field, right side-lines indicate particle trajectories. Normalized times, Ut/a; 18, 55, 112, 175, 217, 280, 340, 418 and 463 correspond to 0.07, 4, 8, 12, 15, 19, 24, 29 and 32 minutes after impact.

TJA97037SFD-1

Collapse of Second Peak Ut/a = 340

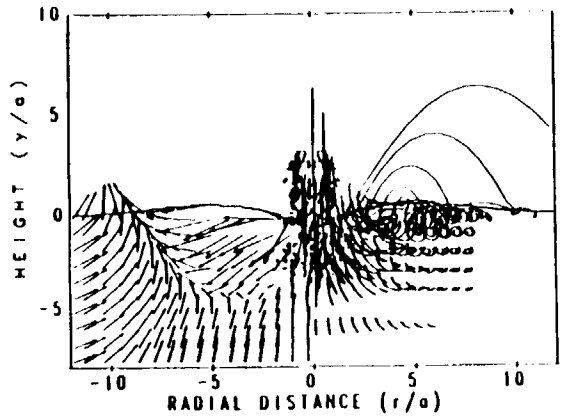

g

Maximum Height of Third Peak Ut/a = 418

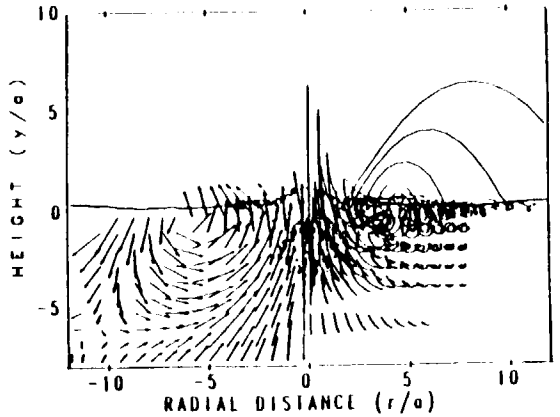

h

Decayed Third Peak Ut/a =463

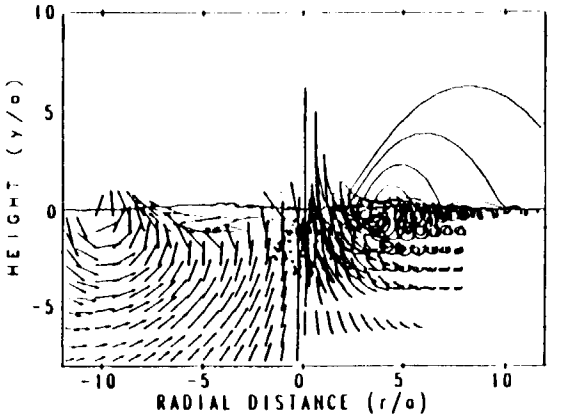

i

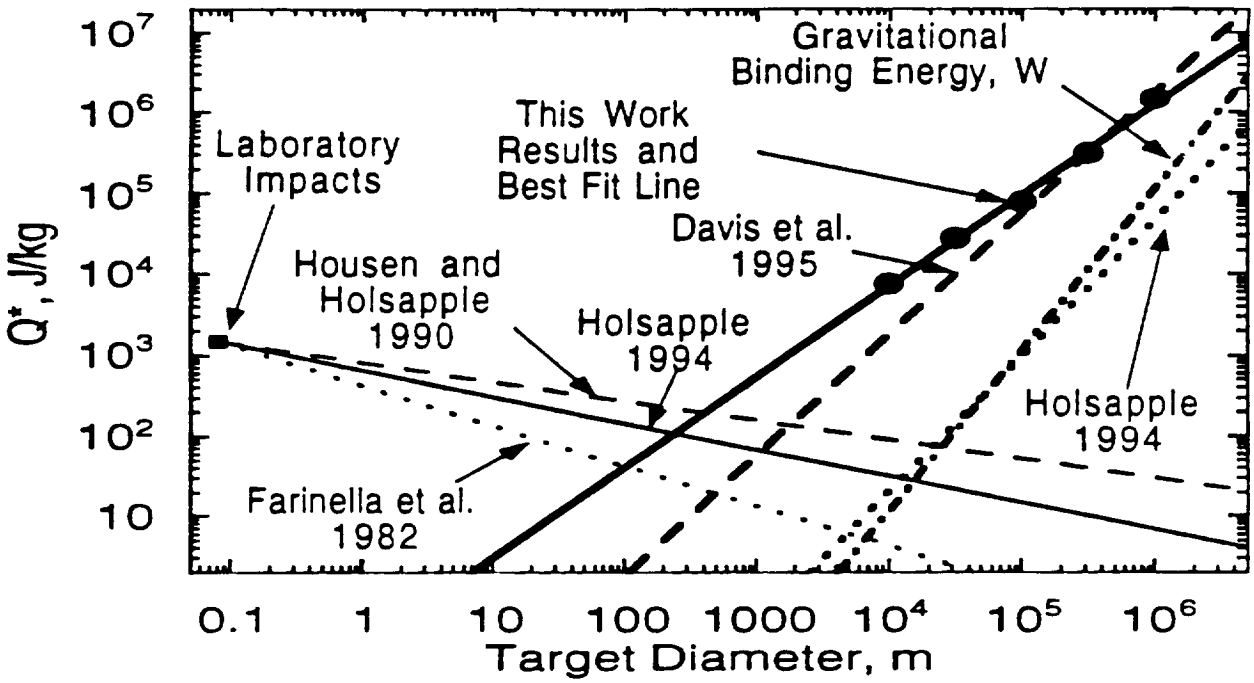

Figure 9 Catastrophic threshold (Q*) as a function of size in the strength (left portion) and gravity (right portion) regimes according to this work and previous studies. In the strength regime we plot Q* for laboratory impact experiments on silicate targets, along with the scaling curves of Farinella et al. (1982), Housen and Holsapple (1990), and Holsapple (1994), with power law slopes of -0.5, -0.24, and -0.33, respectively. In the gravity regime we plot the results of Love and Ahrens (1996) as well as those of Davis et al. (1995) and Holsapple (1994). Love and Ahrens (1996) show the gravitational binding energy, per unit mass, W, is a firm lower limit on Q*. The power law slopes of these relations are respectively 1.13±0.01, 1.5, 1.69, and 2.0. The intersection of the present results with the suite of strength scaling curves indicates that the gravity regime for silicate bodies may begin at diameters as small as 250±150m. (after Love & Ahrens, 1996).

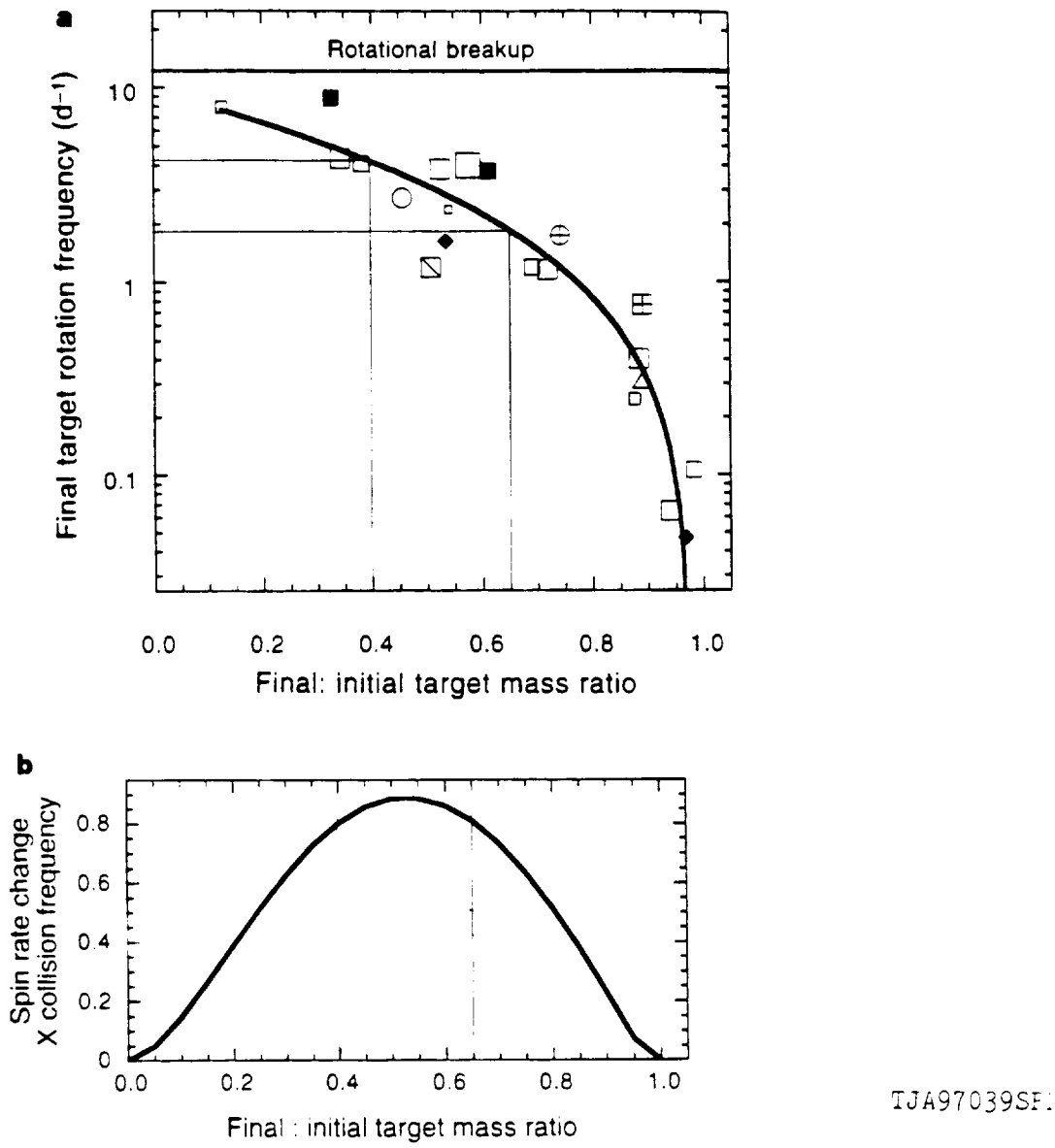

Figure 10 **a**. Final target rotation frequency f as a function of the ratio, μ, of the target's post-impact mass to its initial mass. The unshaded points denote granite targets. Symbols without lines inside represent 45° impacts, crossed symbols 75°, and the slashed symbol 15°. Square symbols denote 5 km s^{-1} impact speed, round 7 km s^{-1} and triangular 3 km s^{-1}. The five different symbol sizes represent from smallest to largest (10 km to 10^3 km) target body diameters. The filled squares represent iron and the filled diamonds dry-tuff targets; these trials employed 100-km targets struck at 5 km s^{-1} and 45°. The final rotation rate does not depend strongly on the absolute target size or on the impact velocity. Grazing and near-vertical impacts yield respectively faster and slower rotation for the same mass loss. The heavy horizontal line marks the 11.9d^{-1} maximum spin rate (corresponding to rotational breakup) for strengthless spherical bodies of density 2,680 kg m^{-3}. The heavy curved line is a fit to the points for 45° impacts. **b**. Relative importance (in arbitrary units, with dimensions of time^{-2}) of impacts of different severity in determining asteroid rotation rate. Shown is the product of the change in spin rate imparted to a target by impacts of various sizes (from the present model) and the relative frequency of such collisions, assuming an asteroid mass-frequency distribution with a power-law slope near -1.7. Collisions that leave target remnants with 0.40-0.65 of their original mass and correspond (according to **a**) to a change in spin frequency of 1.8-4.2d^{-1} control rotation rate evolution (after Love & Ahrens, 1997).

(a)

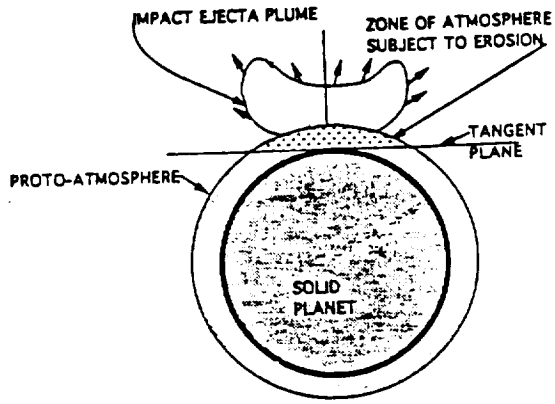

(b)

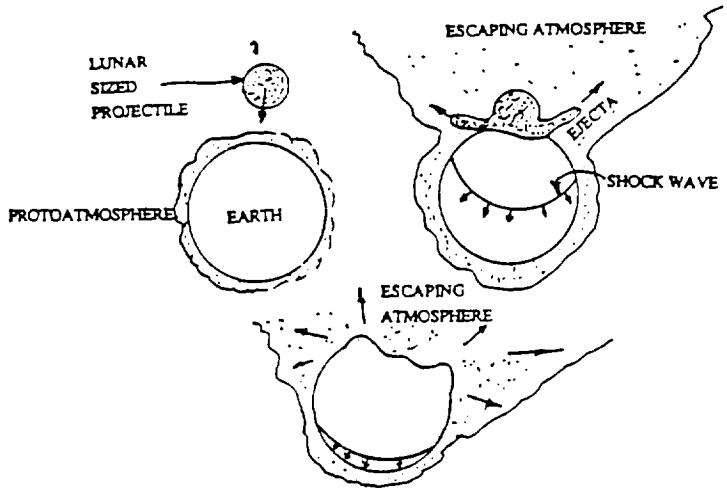

Figure 11 Two proposed modes of impact atmosphere erosion: (a) Atmosphere lying above the plane tangent to the Earth surface at the impact point is blown off by impact generated vapor plume. After Vickery and Melosh 1990. (b) A shock wave propagates through the solid planet and the atmosphere is accelerated by the movement of the planetary surface. After Ahrens 1993.

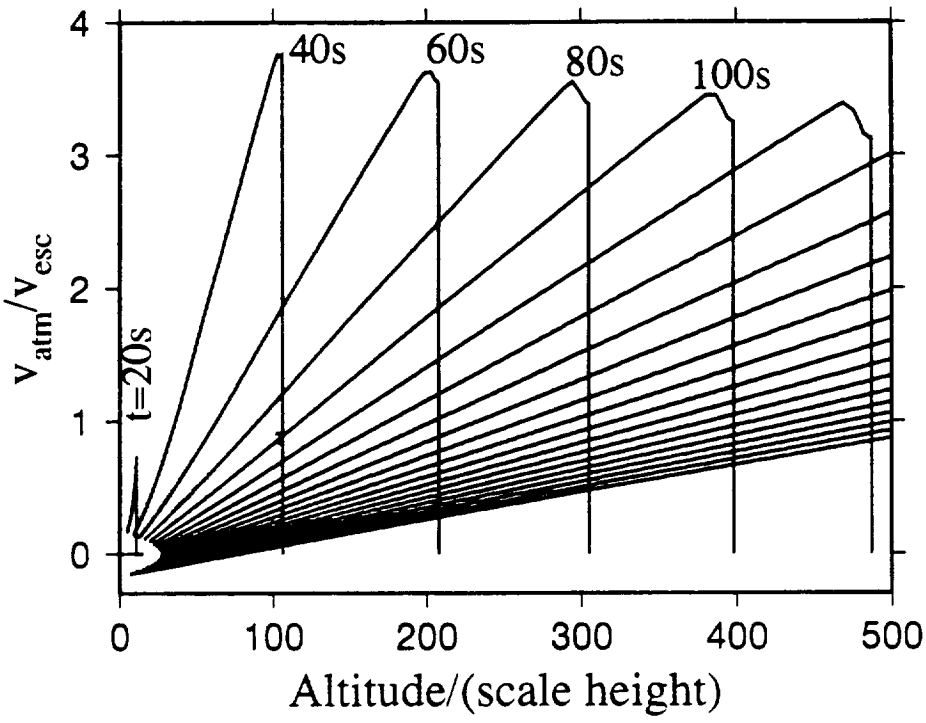

Figure 12. Time history of shock wave profile in the atmosphere. Surface velocity v = 2 km/s, polytropic constant γ=1.40, initial atmosphere thickness in the calculation is 16 times scale height.